Report no. changed (Mar 2006): SM-389-UU

SACLANTCEN MEMORANDUM
serial no: SM- 389

SACLANT UNDERSEA RESEARCH CENTRE REPORT

Real-and synthetic-array signal processing of buried targets

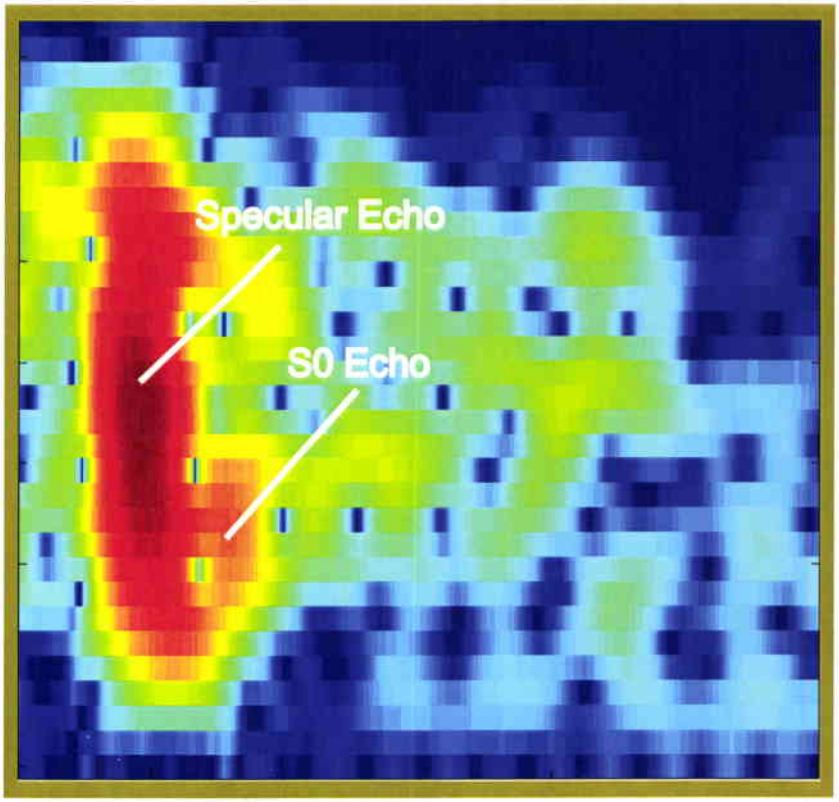

Marc A. Pinto, Andrea Bellettini, Reginald Hollett and Alessandra Tesei

January 2002

NORTH ATLANTIC TREATY ORGANIZATION ORGANISATION DU TRAITE DE L'ATLANTIQUE NORD

Report no. changed (Mar 2006): SM-389-UU

Real– and synthetic–array signal processing of buried targets

M.A. Pinto, A. Bellettini,
R. Hollett, A. Tesei

The content of this document pertains to work performed under Project 03-G of the SACLANTCEN Programme of Work. The document has been approved for release by The Director, SACLANTCEN.

Jan L. Spoelstra
Director

Report no. changed (Mar 2006): SM-389-UU

intentionally blank page

Report no. changed (Mar 2006): SM-389-UU

Real– and synthetic–array signal processing of buried targets

M.A. Pinto, A. Bellettini, R. Hollett, A. Tesei

Executive Summary:

Due to the high absorption of high frequency sound in hard marine sediments (e.g. sand), the usefulness of conventional minehunting sonars for the detection of buried mines is very limited. To reduce this absorption, specific low frequency sonars have to be used. The difficulty is then to maintain sufficient resolution to reduce the seafloor reverberation, which is the background against which the echoes of buried targets have to be detected. Previous work has demonstrated the ability of scanned parametric sonars to detect buried targets, due to their large relative bandwidth and comparatively narrow pencil beams. This report studies the combination of a 2-16 kHz parametric transmitter with two directive receiving arrays. The first is a 12 m horizontal line array and the second a 1.4 m vertical line array which was displaced horizontally to form a synthetic aperture sonar. The transmission beam of the parametric sonar was electronically scanned along-track during the synthetic aperture sonar formation, to increase the length of the synthetic aperture.

Due to the increased directivity in both receiving systems, important gains in detection are obtained, at grazing angles both above and below the critical angle of total reflection. An environmentally adaptive matched filter theory is also developed, which accounts for the change in absorption over the transmitted bandwidth, and shown to provide significant gains over the conventional theory. The high resolution images obtained in both cases allow a straightforward discrimination between buried spherical and cylindrical shells. In addition resonant scattering theory is shown to provide robust additional classification cue for the simpler case of the air-filled spherical shell.

intentionally blank page

Report no. changed (Mar 2006): SM-389-UU

Real– and synthetic–array signal processing of buried targets

M.A. Pinto, A. Bellettini, R. Hollett, A. Tesei

Abstract: Results from two field experiments aimed at investigating the detection and classification of buried targets are presented. In both experiments a 2-16 kHz parametric source was used. In the first experiment the source was used in combination with a 12 m horizontal line array and in the second with a 1.4 m vertical line array which was displaced horizontally along an underwater rail to form a 10 m x 1.4 m two dimensional synthetic aperture sonar (SAS). To increase the SAS integration time, the parametric source was electronically scanned in azimuth during the displacement along the rail, as in spotlight mode. It is shown that both arrays allow important signal to reverberation gains, enhancing the detection of sub-bottom echoes. A new, environmentally adaptive, matched filter which further improves the signal to reverberation ratio while allowing discrimination between proud and buried targets is presented and validated experimentally. The use of resonant scattering for target classification of buried objects is discussed, in the particular case of spherical shells.

Report no. changed (Mar 2006): SM-389-UU

Report no. changed (Mar 2006): SM-389-UU

1

Introduction

Targets may bury into hard marine sediments (e.g. sand) through a number of natural mechanisms, such as scouring due to waves, tides or currents, followed by sediment transport. Targets can also be designed to bury themselves and are then very well hidden to conventional imaging sonars, because at the high frequencies (typically above 100 kHz) and low grazing angles at which these sonars operate, the propagation loss in the sediment reduces the level of a sub-bottom echo well below that of the seafloor reverberation. Above the critical grazing angle of total reflection θ_c, given according to conventional wave theory by $\cos\theta_c = c_w/c_s$, where c_s (resp. c_w) is the sound speed in the bottom (resp. water), the propagation loss relates chiefly to the sediment absorption. Below the critical angle, the sound penetrating in the sediment is evanescent, i.e. decaying exponentially with the burial depth in wavelengths, and the loss is much higher. Thus subcritical detection of buried objects, which is desirable in order to extend the detection range, is a challenging issue.

A buried object sonar must operate at a low enough frequency, to limit the propagation loss in the sediment, while maintaining sufficient resolution, to minimize reverberation. This unusual requirement for high resolution at low frequencies characterizes the buried object detection problem. The resolution can be obtained, as for a conventional imaging sonar, by the use of wideband signals and directive arrays, but this is more difficult to achieve at low frequencies with compact sonar designs.

Parametric sonar is an interesting technology in this context since it can provide wide bandwidth as well as directive pencil beams with relatively small transducers. However, in order to achieve area coverage, it requires scanning, which is more time consuming and involves compromises between resolution, rate of advance, complexity etc. An experimental scanned parametric sonar for buried mine detection has been reported in the military field but little detail has been released in the open literature [1].

Section 2 presents the results of a field experiment based on a 2-16 kHz parametric sonar, together with a 12 m horizontal line array (HLA). In Section 2.1 a new matched filter, suited for buried object detection, is presented and validated using experimental data from the HLA. The detection performance is discussed as a function of grazing angle and burial depth. In Section 2.2 the use of resonant scattering

Report no. changed (Mar 2006): SM-389-UU

theory for buried target classification is discussed, in the particular case of spherical shells. Section 3 presents the results of a second field experiment, based on the same parametric sonar used together with a 1.4 m vertical line array (VLA) in reception. This sonar was displaced horizontally along an underwater rail to form a 10 m x 1.4 m, two dimensional, synthetic aperture sonar (SAS). To increase the SAS integration time, the parametric source was electronically scanned in azimuth during the displacement along the rail, as in spotlight SAS. The theory developed in Section 2.1.1 and 2.2 is applied to the data and the results are presented.

Report no. changed (Mar 2006): SM-389-UU

2

Horizontal line array

The GOATS'98 experiment [2] was conducted jointly by NATO Saclant Undersea Research Centre (SACLANTCEN) and M.I.T. in May 1998, near Marciana Marina, off the island of Elba (Italy) using a parametric source and a variety of receiving arrays, including the 12 m HLA considered here.

The parametric source was a commercial system [3] which consisted of 24 horizontal staves, electronically controlled to form a beam in a selected direction. It operated

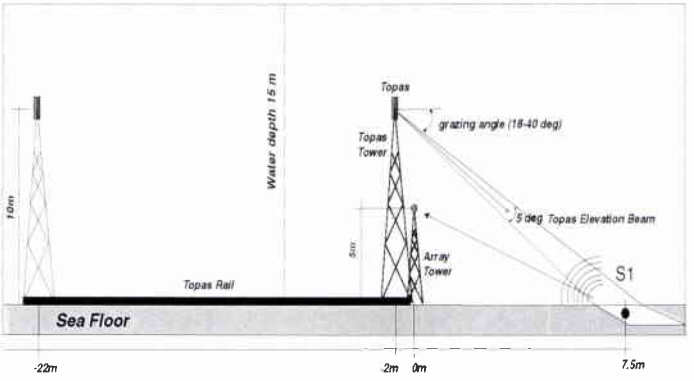

Figure 1 *Layout of the HLA experiment (side view).*

around a primary frequency of 40 kHz with a source level of 238 dB. The secondary source level varied from 190 dB to 213 dB in the 2-16 kHz band. The pulse used was an 8 kHz Ricker wavelet with 6 kHz bandwidth and the beamwidth of the source was 9° in azimuth and 5° in elevation .

To allow ensonification of the target at a wide range of grazing angles, the source was mounted on a 10 m tower, in a pan and tilt assembly with a motion reference unit for precise steering of the source beam. This tower was capable of being displaced along a 24 m rail lying on the seabed. The position of the tower was precisely controlled using an electric motor, remotely controlled from the shore laboratory. The HLA consisted of 128 elements spaced at $\lambda/2$ at 8 kHz, for a total length $L = 12$ m and a 3 dB angular resolution of 0.775° at 8 kHz. It was fixed in the water column, suspended 5 m above the seabed between two trellis towers, at right angles to the rail (Figs. 1-2).

Report no. changed (Mar 2006): SM-389-UU

The analysis of cores provided grain size estimates corresponding to medium sand. The sound speed in the bottom was measured at 1720 m/s at 200 kHz. In the water column an isovelocity profile was measured at 1520 m/s. This gave a critical grazing angle of about 28°, according to conventional wave theory.

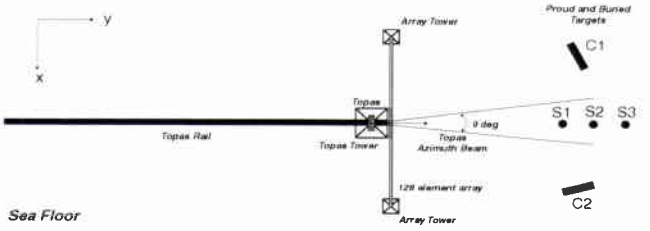

Figure 2 *Layout of the HLA experiment (top view).*

The target field consisted of three identical air-filled spherical shells S1, S2 and S3 deployed in line with the rail, spaced by 5 m. The spheres were of 1.06 m outer diameter and 3 cm shell thickness. The burial depth, measured from the centre of the sphere was 0.9 m (resp. 0.5 m, 0 m) for S1 (resp. S2, S3). The rationale behind having three spheres and the underwater rail was to be able to evaluate detection performance as a function of grazing angle and burial depth. The transmission grazing angle varied according to the tower position and the target to ensonify. The reception grazing angle was fixed for each target, because displacing the HLA was not practical. For example, the sphere S1 had a transmission grazing angle θ_i varying between 18° and 40°, depending on the tower position, and a fixed reception grazing angle $\theta_r \approx 34°$. In addition two identical steel cylinders C1 and C2 were deployed with different orientations to the rail. The cylinders were 2 m long and 0.5 m in diameter. The shell thickness was 6 mm and both cylinders were filled with seawater and flush buried in the sediment (i.e. just below the seabed).

2.1 Detection of buried targets

2.1.1 Environmentally adaptive matched filter

Let $S(f)$ be the spectrum of the transmitted pulse, extending from f_1 to f_2, $S(f)A(f)$ the spectrum of the sub-bottom echo and $N(f) = |S(f)|^2 N_r(f)$ the spectral density of the reverberation signal at the sensor output, where $N_r(f)$ is the spectral density of the backscatter. At the output of a receiving filter $R(f)$, for a delay matched to

Report no. changed (Mar 2006): SM-389-UU

that of the sub-bottom echo, the signal to reverberation ratio ρ can be expressed as

$$\rho = \frac{|\int_{f_1}^{f_2} R(f)A(f)S(f)df|^2}{\int_{f_1}^{f_2} |R(f)|^2 N(f)df} \tag{1}$$

Then, it is a classical result of signal theory [4] that the optimal filter $R_{opt}(f)$, i.e. the filter which maximises ρ is given by

$$R_{opt}(f) = \frac{A^*(f)S^*(f)}{N(f)} \tag{2}$$

and the corresponding ρ_{opt} is

$$\rho_{opt} = \int_{f_1}^{f_2} \frac{|A(f)S(f)|^2}{N(f)} df = \int_{f_1}^{f_2} \frac{|A(f)|^2}{N_r(f)} df \tag{3}$$

These equations are not new, but to our knowledge they have never been used in buried target detection.

A very simple signal model for the sub-bottom echo is $|A(f)| = Ae^{-\alpha f}$, where A and α are constants. The parameter α depends on the length of the two-way travel path in the sediment and the mechanism for propagation loss in the sediment. Above the critical angle, this is the absorption in the sediment, of the order of 0.5 dB/λ for the bottom type investigated here, whereas below the critical angle it relates chiefly to penetration loss due to conversion into evanescent sound. More sophisticated target and propagation models could also be introduced. These would allow higher detection gains but would probably be more sensitive to model mismatch.

If it is assumed in addition that the spectrum of the transmitted signal and the backscatter are flat from f_1 to f_2, i.e. $|S(f)| = S$, $N_r(f) = N_r$, where S and N_r are constants, then

$$|R_{opt}(f)| = \frac{A}{SN_r} e^{-\alpha f} \tag{4}$$

as well as

$$\rho_{opt} = \frac{A^2}{N_r} \int_{f_1}^{f_2} e^{-2\alpha f} df = \frac{A^2}{N_r} \frac{e^{-2\alpha f_1}(1 - e^{-2\alpha B})}{2\alpha} \tag{5}$$

where $B = f_2 - f_1$ is the signal bandwidth. The conventional proud target case corresponds to $\alpha = 0$ in which case $\rho_{opt} = A^2 B/N_r$. We have then the familiar result that ρ_{opt} is independent of centre frequency and increases linearly with bandwidth B. It is this result which motivates the use of wideband signals for improved detection of proud targets with low target strength. The case $\alpha > 0$ is remarkably different since ρ_{opt} increases, for fixed B, when f_1 is reduced. In addition, while it remains true that ρ_{opt} increases with B, the increase is highly non-linear: the gain becomes negligible as soon as $B \gg 1/2\alpha$ and the quantity $A^2/(2\alpha N_r)$ sets an upper bound on the achievable ρ_{opt}. Thus the efficiency of wideband operation, in enhancing buried target detection, is reduced compared to proud targets.

2.1.2 Experimental validation

The experimental results for S1, after complex demodulation and before matched filtering, are shown in Fig. 3 in the quasi-monostatic case for which $\theta_i = \theta_r \approx 34°$, where θ_i and θ_r are the transmitter and receiver grazing angles. Since the HLA operated deep in the near field (the Fresnel distance $L^2/\lambda = 768$ m at 8 kHz), a focused wideband beamformer was used. The beamformer did not take the refraction into the sediment into account. The mean reverberation level was computed using order truncated averaging and is plotted in Fig. 3 together with the curve 12 dB above it, where 12 dB was chosen as a typical value of the signal excess. It is seen that the beamformer gain in the signal to reverberation ratio (SRR) is 5 dB. A

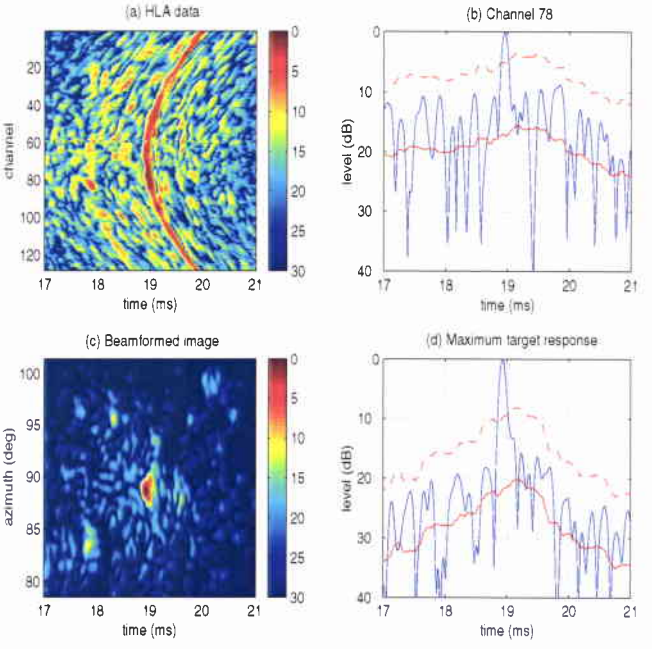

Figure 3 *Experimental results for sphere S1: envelope of HLA data (a), envelope of channel 78 (b), beamformed image (c) and beam of maximum target response (d). The red curve shows the mean reverberation level and the dashed one is 12 dB above it. The grazing angles are* $\theta_i = \theta_r \approx 34°$.

difficulty in applying the above matched filter theory is that the value of α depends on the range and depth of the possible targets and therefore is not known in advance. The solution is to apply a bank of matched filters, parameterized by possible values of α, to the experimental data and to retain, for each delay matched to that of a possible sub-bottom echo, the value of α which maximises the power at the filter output. The experimental results are shown in Fig. 4 for the filter bank

$$R_\alpha(f) = C_\alpha e^{-\alpha f} \tag{6}$$

where

$$C_\alpha = \left(\frac{2\alpha}{e^{-2\alpha f_1}(1 - e^{-2\alpha B})} \right)^{1/2} \tag{7}$$

C_α is chosen so that $\int_{f_1}^{f_2} |R_\alpha(f)|^2 df = 1$. Thus, for the simple signal model described above, the power in the reverberation at the output of all the filters in the bank does not depend on α. The target and reverberation levels were computed at the output of the HLA beam steered towards the target, i.e. giving maximum target amplitude.

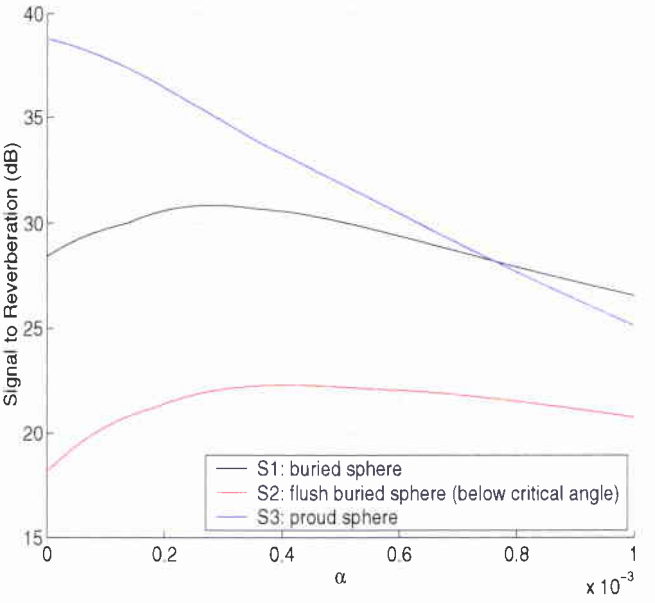

Figure 4 *Experimental signal to reverberation ratio of the three spheres for the continuous bank of filters of Eq. (6). For the buried sphere S1 both transmission and reception grazing angles are nearly equal ($\theta_i = \theta_r \approx 34°$) and above the critical angle $\theta_c \approx 28°$. In the case of the flush-buried sphere S2 the transmission is above the critical angle ($\theta_i \approx 30°$) but reception is below ($\theta_r \approx 22°$).*

It is seen in Fig. 4 that for the half-buried sphere S3, the measured SRR decreases with $\alpha > 0$ from a maximum attained for $\alpha = 0$. This is the expected behaviour for a proud target. It would seem from the data that the SRR would be even greater for $\alpha < 0$, i.e. for a filter which would emphasize the higher frequencies. This is probably because the spectrum of the transmitted pulse is not flat as assumed in the simple signal model.

For the buried sphere S1 (resp. S2) there is an optimal positive value of α, equal to $\alpha = 2.8 \cdot 10^{-4}$ (resp. $\alpha = 4 \cdot 10^{-4}$). A higher value of α is expected for S2 than for S1 because for S2 the reception angle is about 22°, which is below the critical angle. For S2, the gain in SRR of the adaptive signal processing over the conventional processing, which corresponds to $\alpha = 0$, is more than 3 dB. This is a large gain in

Report no. changed (Mar 2006): SM-389-UU

this reverberation-limited situation.

2.1.3 Grazing angle dependence

The deeply buried sphere S1 was buried in such a way that the grazing angle in reception θ_r was above critical and equal to 33°. The SRR for S1 is plotted as a function of transmission grazing angle θ_i in Fig. 5, for various α as well as the optimized SRR, obtained by maximizing over α. It is seen that the SRR increases monotonically with the grazing angle for small α, but shows a maximum for large α, for a value of the grazing angle which is close to the critical angle $\theta_c \approx 28°$ [1]. The monotonic increase with grazing angle for small α, as well as for large α below the critical angle, is due to the reduction in the attenuation in the sediment. This attenuation is high for small α (i.e. high frequency) at all grazing angles, as well as for large α (i.e. low frequency) below the critical angle. For large α, above the critical angle, the attenuation in the sediment is low and the decrease in SRR is probably due to the increase in the reverberation level with grazing angle. The optimum SRR is seen to be a monotonic function of grazing angle.

The deeply buried sphere S1 is detected with a signal excess of at least 15 dB for all grazing angles greater than 18°. This is an encouraging result. Two points, however, warrant attention. The first is that the target strength of some targets (e.g. mines), may be significantly lower than that of a 1 m diameter spherical shell, with a corresponding lowering of the signal excess in Fig. 5. The second is that the experimental data were gathered in a favourable bistatic case. The signal excess could be much lower when both the transmission and reception grazing angles are reduced, as required to maximise the detection range. Then the propagation loss for the travel from the target back to the receiver would increase when θ_r is reduced, rather than being constant as in Fig. 5.

2.1.4 Beamforming results for buried targets

Different low pass filters were applied to the beamformed HLA data as an approximate means of applying the above detection theory (Fig. 6). The white shapes show the estimated positions of the targets, computed from the geometry of the experiment. These are seen to be offset from the real positions for reasons discussed in Section 2.1.3. The specular echoes from S1, as well as from the front face and the back face of C1, are clearly detected. Many other contacts are visible in the top

[1] The slight difference could be due to measurement errors in the geometry of the experiment, for which the grazing angle is computed. It is apparent in Fig. 6 that the targets are at horizontal ranges which are larger by 1-2 m than the measured values. Thus it is likely that the actual grazing angles are slightly smaller than those computed from Fig.1.

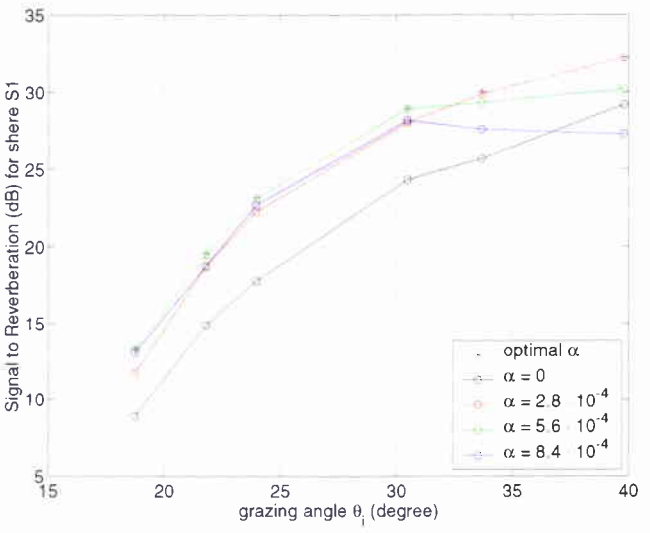

Figure 5 *Signal to reverberation ratio for buried sphere S1 in function of transmission grazing angle and filter parameter α. Reception grazing angle is $\theta_r \approx 34°$.*

right images. The SRR for S1 is emphasized by the low-pass filtering, in agreement with expectations. The same holds for C1 which indicates that the theory can be applied with benefit also to targets whose strength varies significantly over the signal bandwidth. In addition in the bottom left image, a second resonant echo behind the specular echo from the sphere is clearly apparent. The level of the other contacts are seen to recede into the background reverberation as the low-pass filtering is applied. This is the behaviour predicted for proud targets by the above detection theory. In addition these may be objects of smaller dimension whose target strength decreases with frequency.

2.2 Classification of buried targets

Classification is an important open problem for buried objects. For proud targets, imaged with high resolution sonar, classification clues are based on the structure of both the target echo and that of the acoustic shadow cast on the seafloor. Since there is no acoustic shadow for buried targets, the classification must be based on the echo structure alone. It is apparent in Fig. 6 that the specular echoes have the capacity to provide important classification clues. In particular it is seen that the length of the cylinder C1, which is equal to 2 m, can be accurately estimated from the beamformed data. Resonant echoes, when present, as in the bottom left image of Fig. 6, provide additional classification clues.

Only the response of the buried sphere S1 is analyzed in what follows. The echo

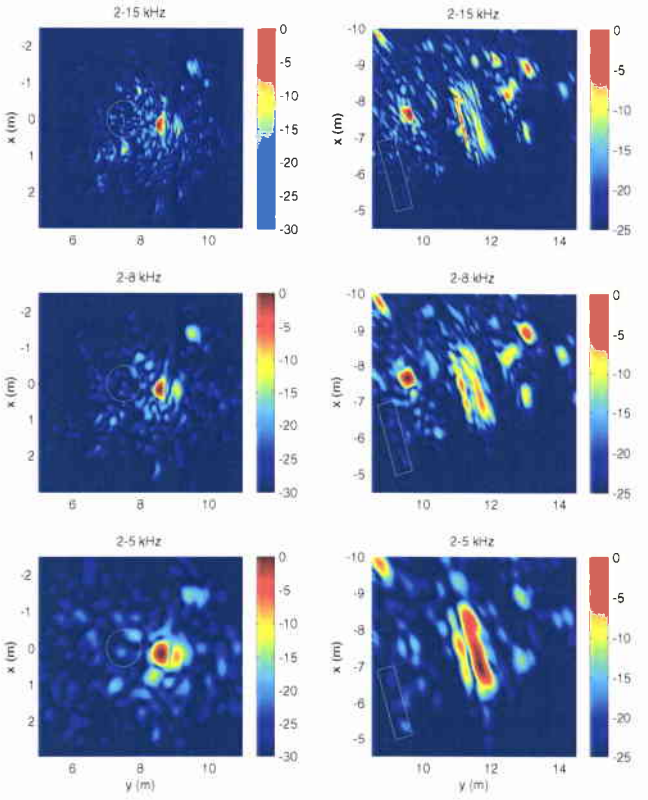

Figure 6 *Beamforming results for buried sphere S1 and buried cylinder C1 with different low-pass filters. The white shapes show the actual size and estimated position of the targets, using the geometry of the experiment. The grazing angles are* $\theta_i = \theta_r \approx 34°$ *for the sphere and* $\theta_i \approx 24°$, $\theta_r \approx 25°$ *for the cylinder.*

received by each of the 128 hydrophones of the HLA is modelled in the frequency range (0,12) kHz by means of a T-matrix-based simulator developed by Lim et al. ([5],[6]).

The raw data and beamformed image of the model (Fig. 7) show, in addition to the sphere's specular echo, two main families of elastic surface waves [7].

The S_0 Lamb-type wave is quasi non-dispersive, supersonic, and circulates around the spherical shell in the sediment-shell interface with a phase speed corresponding to the shell material membrane speed ($c^* = 5435$ m/s for steel). Due to the perfect 3D symmetry of the object shape, the wave reradiates at each revolution in all directions with an angle corresponding to the shell material critical angle. Each echo outlined in Fig. 7 is the result of the superposition of two sets of simultaneous wave echoes, one generated by a wave travelling clockwise around the sphere and the other generated by an identical wave travelling anticlockwise. In backscattering, the two echoes are perfectly superimposed as they arrive at the receiver at the same time.

As the azimuth angle changes from the backscattering direction, the interference between the two echoes becomes more and more destructive as the echoes travel along increasingly different paths. This explains the fading effect observable in the model envelope (Fig. 7(a)) at angles far from the backward direction. However, due to the target shape symmetry and the relatively low-frequency composition of the S_0 wave, the spatial coherence of the S_0 Lamb-type wave extends over a wide azimuth sector. Hence, for example, the level of the first S_0 echo is about 12 dB less than the specular echo on the backward channel, and slowly decreases as the azimuth angle varies.

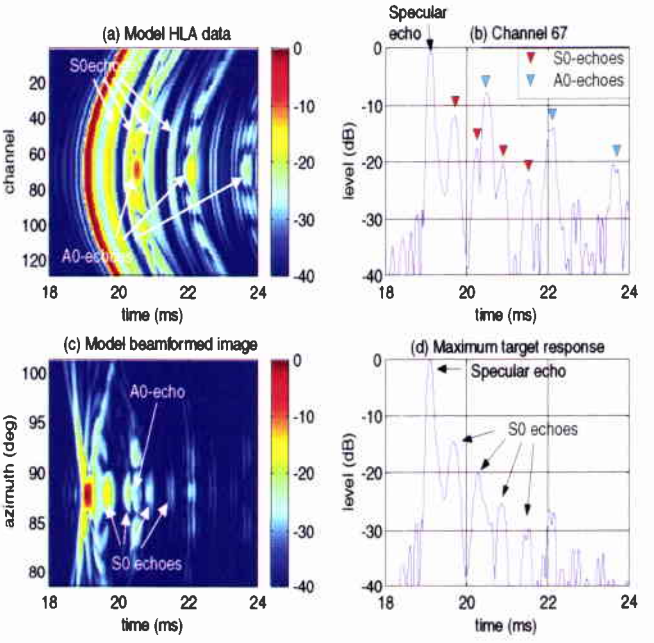

Figure 7 *Model results for sphere S1: envelope of HLA data (a), envelope of channel 67 (b), beamformed image (c) and beam of maximum target response (d).*

The A_{0-} Lamb-type surface wave is the other wave family which can be identified from the sphere scattering model. The wave is dispersive, subsonic, more readily observed when the wave phase speed approaches the outer-medium sound speed, and reradiates at each revolution approximately along the tangent to the sphere cross-section. As for the S_0 wave, each echo identified in the time-azimuth plane derives from the superposition of two echo families which are perfectly superimposed over an azimuth range around the backward direction, but interfere destructively beyond this range (see Fig. 7(a)). Compared to the S_0 wave, due to the higher frequency composition of the A_{0-} wave, even a slight difference in the times of arrival of the two echoes causes an evident destructive interference. Hence the A_{0-} wave azimuthal coherence is restricted to a narrower angular range than for the S_0 wave.

The different nature of the two waves in terms of spatial coherence explains the

result of the beamforming (Fig. 7). There is a loss in array gain of about 3 dB for the S_0 wave first echo compared to the specular echo. The loss for the A_{0-} wave is much higher due to its spatial incoherence.

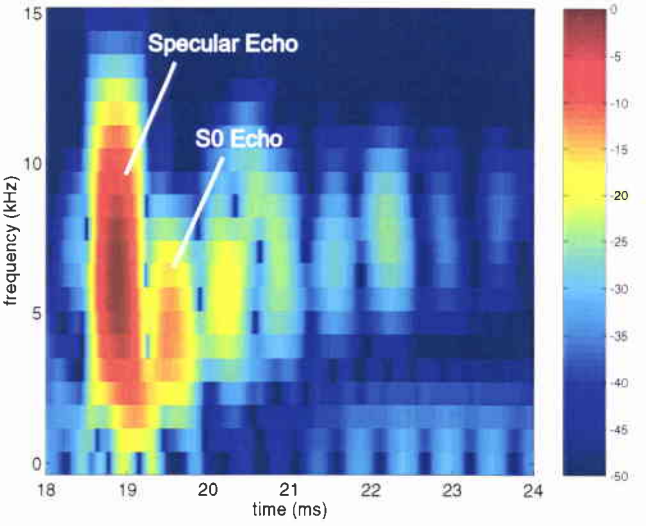

Figure 8 *Model results: spectrogram of the maximum target response after beamforming, filtered in the range (1,12) kHz.*

The spectrogram of the modelled beam steered toward the target is shown in Fig. 8. The representation describes the frequency composition of the echoes. In particular, the S_0 first two echoes spread over the frequency range (2, 8) kHz. As a consequence, in order to increase the detectability of certain wave echoes, the data should be filtered over the most appropriate bandwidth for that wave.

Only the S_0 first echo is clearly detectable after the specular echo. Its main contribution is between 3 and 7 kHz, hence a bandpass filter was applied to the raw data in this frequency range and the result is presented in Fig. 9. Now the array gain on the S_0 first echo vs. the residual reverberation level is 22 dB. The spectrogram was also computed for the experimental data (Fig. 10).

In conclusion, with respect to single-aspect monostatic measurement of the target response, the use of a long HLA improves the detectability of both the target specular echo and those elastic features that are spatially coherent for a wide range of azimuth angles.

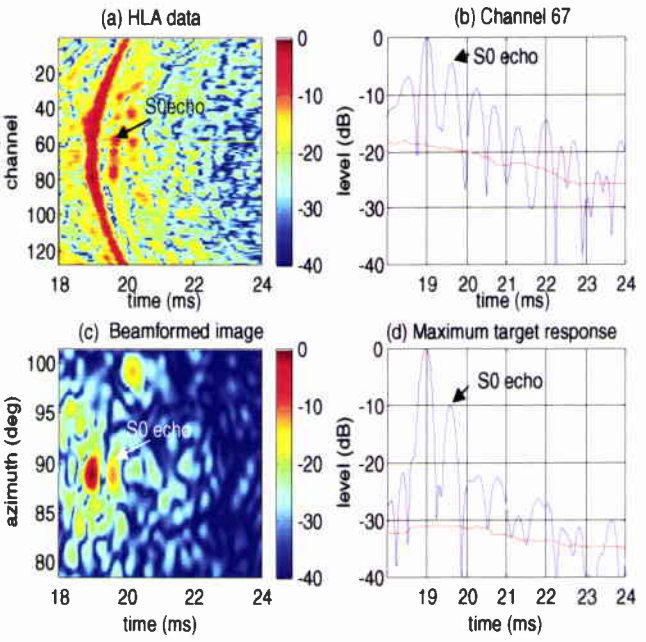

Figure 9 *Experimental results for sphere S1 filtered in the frequency range (3,7) kHz: envelope of HLA data (a), envelope of channel 67 (b), beamformed image (c) and beam of maximum target response (d). The red curve shows the average reverberation level. The grazing angles are* $\theta_i = \theta_r \approx 34°$.

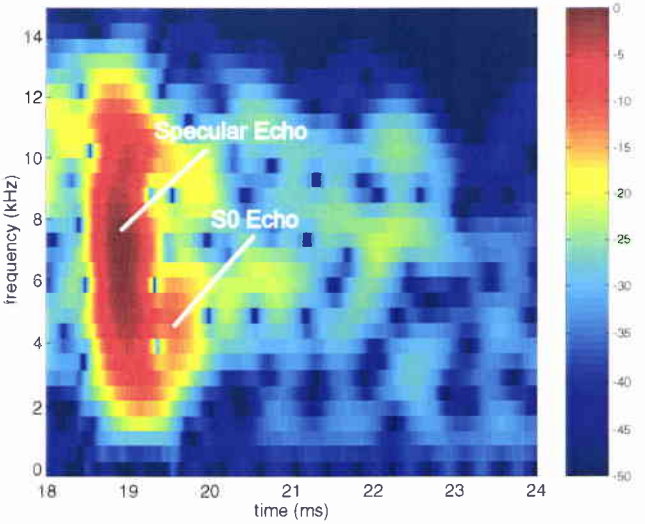

Figure 10 *Experimental results: spectrogram of the maximum target response after beamforming, filtered in the range (1,12) kHz.*

Report no. changed (Mar 2006): SM-389-UU

3

Spotlight parametric synthetic aperture sonar

A joint experiment between Saclantcen and GESMA (Groupe d'Etudes Sous-Marines de l'Atlantique), France was performed in November 1999, at the Lanvéoc underwater rail facility in the Brest (France) area. This facility consisted of a 12.5 m I-beam which was capable of being lowered to seven different heights above the seabed, separated by 0.985 m. The fourth level, which was also the reference level for the tides, was approximately 9 m above the seafloor. An isovelocity profile of 1500 m/s was observed at in the water column. The seabed type was complex and inhomogeneous, consisting of dead marl which is decomposed into finer and finer grains as the depth into the sediment increases. Significant gas content was observed, probably related to biological activity. The sound velocity showed wild variations with depth in the sediment and position of the cores. The mean value was close to that in water, indicating the probable absence of critical angle for this bottom type.

A trolley, capable of carrying payloads up to 500 kg, was displaced at controlled speed along the rail. The parametric source described above was mounted together with a vertical line array on a tilt assembly, which in turn was mounted on the trolley. The source was mounted horizontally, instead of vertically as in the HLA experiment, giving a 3 dB beamwidth of 5° azimuth and 9° in elevation. The transmitted signal was a 5 ms LFM, swept from 2 kHz to 10 kHz, in order to increase the energy in the signal and overcome the noise generated by the trolley motion system. The vertical line array (VLA) featured 16 elements spaced at $\lambda/2$ at 8 kHz.

The main objective of this experiment was to examine the feasibility of SAS, as a alternative to the HLA used previously. The use of SAS in place of a HLA leads to a more compact sonar design which is attractive in the context of possible future use on unmanned underwater vehicles (UUVs). In addition the use of a VLA as a physical aperture for SAS allows the synthesis of a 2D receiver array. This array is superior to an HLA because its elevation directivity allows multipath to be resolved.

The combination of SAS with a parametric source is not new [3]. The main advantage of a parametric source, when used in combination with SAS, is the wide bandwidth at low frequency, which is not readily available with compact linear sources. A major disadvantage, however, is that the narrow beam of the parametric source in azimuth limits the length of SAS and hence the resolution gain. To overcome this limitation it was initially considered to continuously steer the parametric beam on

Report no. changed (Mar 2006): SM-389-UU

a selected target, using the electronic scanning capability of the parametric sonar. However a more general mode of operation was preferred. The parametric source was periodically scanned in azimuth, from $-15°$ to $+15°$ by steps of $1°$, during its displacement along the rail. This effectively "spotlighted" all the targets in the field of view. The ping repetition period was only 1 Hz, due to limitations in the data acquisition. This restricted the speed of the displacement to 1 cm/s, giving a total of 1120 pings per run. This SAS mode presented an along-track resolution constant with range and increasing with frequency, approximately equal to 0.8 λ, i.e. 15 cm at 8 kHz. The SAS length was limited by that of the rail, which is close to 11 m, beyond a range of 21 m.

The narrow transmission beam, without sidelobes, allowed a high level of rejection of the azimuth grating lobes of the SAS, thus relaxing the SAS spatial sampling constraint. This situation was the reverse of the usual one, for which a wide sector transmitter is used in conjunction with a set of narrow receive beams formed with a multi-element array.

The field of buried targets deployed for the experiment included a metallic cylindrical shell, 2 m in length and 0.5 m in diameter, and a partly buried spherical shell of diameter 1 m. The cylinder was partly filled with concrete and partly with sand. It was flush buried and was partly visible on a video survey performed using an Sea Twin ROV operated by GESMA. Figure 11 shows the beamformed SAS data, formed at various intermediate stages during the displacement of the sonar on the rail. In this beamforming, only the top 8 elements of the VLA were used to form a vertical beam steered towards the seafloor. The cylinder and the sphere are clearly detected at 13.5 m and 18.5 m. The length of the cylinder, which is 2 m, can be accurately estimated from the beamformed data. A surface-bounced echo from the cylinder, seen through the sidelobes of the VLA, is also apparent at 16 m. It is seen that there are a lot of other contacts between 15 m and 18 m. Divers, as well as a video survey, confirmed the presence of a lot of clutter (cables, wooden beams, etc.) in the vicinity of the buried cylinder.

The same low-pass filters as applied to the HLA were applied to the SAS data and the results are presented in Fig. 12. The benefits of the low-pass filtering are not obvious here, pobably because both targets are partly buried. On the other hand the other contacts between 15 m and 18 m range seem to recede in the background reverberation. It is likely that these are objects of smaller characteristic dimensions which lead to a decreased target strength after low-pass filtering.

An expanded image of the partly buried sphere is shown in Fig. 13. A second echo is clearly apparent at approximately 35 cm behind the specular echo, which corresponds to the S_0 wave. Its level is about 8 dB below the secular echo. Unlike the case shown in Fig. 10, the spectrum of the S_0 echo in Fig. 14 shows no low-pass filtering effect, due to the spherical symmetry of the problem causing no loss in

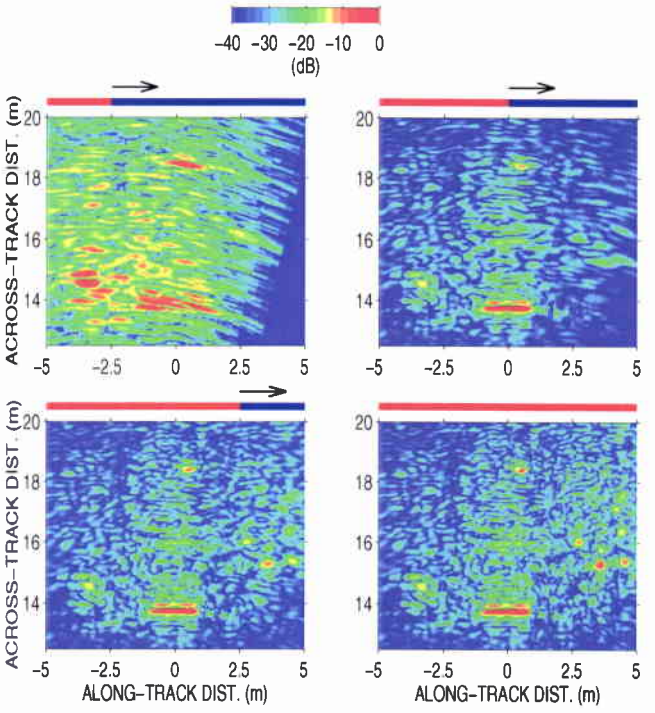

Figure 11 *Beamformed data at various intermediate stages of the spotlight SAS processing. A buried cylinder at 13.5 m and a partly buried sphere at 18.5 m are apparent. Progress along the rail is indicated by the bars above the images.*

spatial coherence.

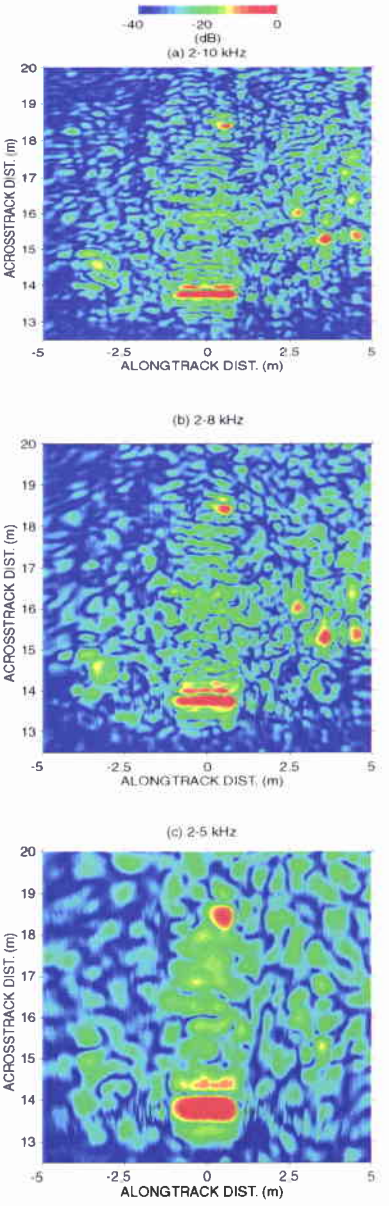

Figure 12 *Spotlight SAS beamformed data for a buried cylinder and a buried sphere with different low-pass filters.*

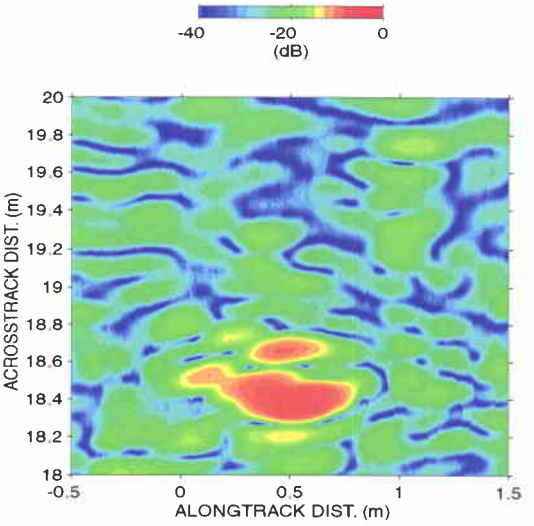

Figure 13 *Spotlight SAS beamforming data for a partly buried sphere filtered in the 2-10 kHz bandwidth, showing specular echo and a resonant echo 35 cm behind.*

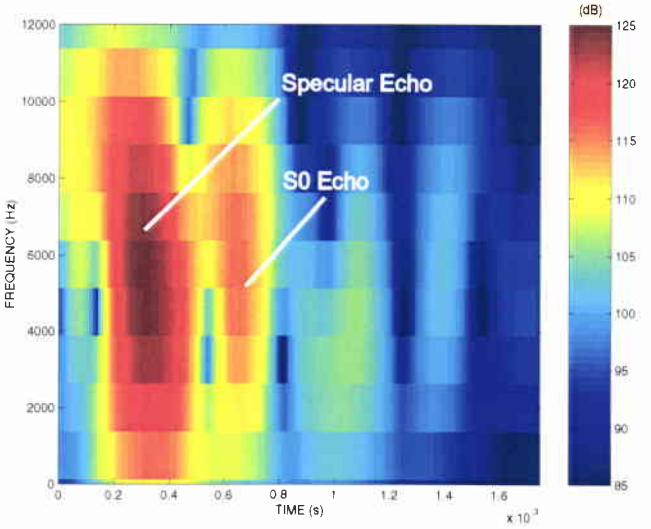

Figure 14 *Spotlight SAS experimental results for a partly buried sphere: spectrogram of the maximum target response after beamforming.*

Report no. changed (Mar 2006): SM-389-UU

4

Conclusion

This paper has shown that successful detection of buried objects through the sediment can be performed at low frequency, using a parametric sonar in combination with real and synthetic arrays. The array processing has been shown to provide important gains in signal to reverberation ratios which are useful both for detection and classification of buried targets, in particular the extraction of resonant classification features of lower target strength. It has also emphasized that the sediment low-pass filters the echoes of buried targets and that this must be taken into account in the temporal signal processing, i.e. the matched filter, to maximise detection.

Report no. changed (Mar 2006): SM-389-UU

Acknowledgments

The authors are grateful to H. Schmidt, scientist in charge of the GOATS'98 experiment, as well as to A. Maguer, W. Fox, E. Bovio, M. Mazzi and M. De Grandi, who contributed greatly to its success. They would also like to express their thanks to A. Hetet (GESMA) and coworkers, for successfully hosting the parametric SAS experiment. Finally, both experiments could not have been performed without the professional support provided by the Engineering and Technology Department of SACLANTCEN, in particular P. Guerrini, P.A. Sletner and coworkers.

Report no. changed (Mar 2006): SM-389-UU

References

[1] Bugler, D. R. Interaction of non-linear acoustics with sediments. *Proceedings of the Institute of Acoustics*, **14**, 1992: 145–159.

[2] Schmidt, H., Maguer, A., Bovio, E., Fox, W. L. J., LePage, K., Pace, N. G., Guerrini, P., Sletner, P. A., Michelozzi, E., Moran, B. and Grieve R. Generic Oceanographic Array Technologies (GOATS)'98 – Bi-static seabed scattering measurements using autonomous underwater vehicles, SACLANTCEN SR-302. La Spezia, Italy, NATO SACLANT Undersea Research Centre, 1998.

[3] Fioravanti, S., A. Maguer, A. and Løvik, A. A synthetic aperture parametric sonar detection of buried targets. In: Proceedings UDT 1996, London, 2-4 July, 1996: pp 198–201.

[4] Rihaczek, A. Principles of high resolution radar, Los Altos, CA, Peninsula Publishing, 1985.

[5] Lim, R., Lopes, J. L., Hackman, R. H. and Todoroff, D. G. Scattering by objects buried in underwater sediments: Theory and experiment. *Journal of the Acoustical Society of America*, **93**, 1993: 1762–1783.

[6] Tesei, A., Maguer, A., Fox, W. L. J., Lim, R. and Schmidt, H. Measurements and modeling of acoustic scattering from partially and completely buried spherical shells. *Journal of the Acoustical Society of America*, submitted 2001.

[7] Sammelmann, G. S., Trivett, D. H. and Hackman, R. H. The acoustic scattering by a submerged, spherical shell. I: The bifurcation of the dispersion curve for the spherical antisymmetric Lamb wave. *Journal of the Acoustical Society of America*, **85**, 1989: 114–124.

Report no. changed (Mar 2006): SM-389-UU

Document Data Sheet

Security Classification		Project No.
UNCLASSIFIED		03-G
Document Serial No.	**Date of Issue**	**Total Pages**
SM-389	January 2002	27 pp.

Author(s)

Pinto, M.A., Bellettini, A., Hollett, R., Tesei, A.

Title

Real-and synthetic-array signal processing of buried targets

Abstract

Results from two field experiments aimed at investigating the detection and classification of buried targets are presented. In both experiments a 2-16 kHz parametric source was used. In the first experiment the source was used in combination with a 12 m horizontal line array and in the second with a 1.4 m vertical line array which was displaced horizontally along an underwater rail to form a 10 m x 1.4 m two dimensional synthetic aperture sonar (SAS). To increase the SAS integration time, the parametric source was electronically scanned in azimuth during the displacement along the rail, as in spotlight mode. It is shown that both arrays allow important signal to reverberation gains, enhancing the detection of sub-bottom echoes.

A new, environmentally adaptive, matched filter which further improves the signal to reverberation ratio while allowing discrimination between proud and buried targets is presented and validated experimentally. The use of resonant scattering for target classification of buried objects is discussed, in the particular case of spherical shells.

Keywords

Issuing Organization

North Atlantic Treaty Organization
SACLANT Undersea Research Centre
Viale San Bartolomeo 400, 19138 La Spezia, Italy

[From N. America: SACLANTCEN (New York) APO AE 09613]

Tel: +39 0187 527 361
Fax:+39 0187 527 700

E-mail: library@saclantc.nato.int

The SACLANT Undersea Research Centre provides the Supreme Allied Commander Atlantic (SACLANT) with scientific and technical assistance under the terms of its NATO charter, which entered into force on 1 February 1963. Without prejudice to this main task - and under the policy direction of SACLANT - the Centre also renders scientific and technical assistance to the individual NATO nations.

This document is approved for public release.
Distribution is unlimited

SACLANT Undersea Research Centre
Viale San Bartolomeo 400
19138 San Bartolomeo (SP), Italy

tel: +39 0187 527 (1) or extension
fax: +39 0187 527 700

e-mail: library@saclantc.nato.int

NORTH ATLANTIC TREATY ORGANIZATION